1st Latin-American Workshop on Structural Health Monitoring
LATAM-SHM 2023
December, 5-8 2023

EXPERIMENTAL ANALYSIS OF THE REFLECTION BEHAVIOR OF ULTRASONIC WAVES AT MATERIAL BOUNDARIES

Jonathan Liebeton and Dirk Söffker

Chair of Dynamics and Control
University of Duisburg-Essen
Campus Duisburg, 47057 Duisburg, Germany
e-mail: jonathan.liebeton@uni-due.de, soeffker@uni-due.de

Key words: Acoustic Emission, wave propagation, signal analysis, reflection, mode

Abstract. Structural Health Monitoring of systems and especially material-based components is often based on the analysis of ultrasonic waves, using active guided wave approach as well as the passive Acoustic Emission approach allowing in-situ non-destructive testing. The properties of ultrasonic waves change depending on their propagation path, particularly affecting amplitude and frequency. Frequency, frequency changes, as well as frequency distributions are commonly used as features to classify damage mechanisms. Modes can serve as an additional damage indicator to distinguish between different damage mechanisms and provide a more precise estimation of propagation velocity. Therefore, these two parameters, frequency and mode, directly influence classification and localization results. In this contribution, the reflection behavior of Lamb waves in carbon fiber reinforced plastic specimen is analyzed. The influence of boundary conditions on reflections is investigated by varying these conditions. Finally, a novel approach of automated reflection and mode detection as well as isolation is presented based on time-frequency and correlation analysis. The isolation of relevant signal parts is based on detecting local maxima in the time-frequency domain. The experimental results provide new insights into the propagation behavior of ultrasonic waves and their reflections at material boundaries, showing a decreasing frequency with an increasing number of reflections. The result is helpful to interpret reflections and understand the behavior of Lamb waves at material boundaries.

1 INTRODUCTION AND LITERATURE REVIEW

In Structural Health Monitoring (SHM) non-destructive testing and evaluation is used to analyze the health of systems, structures, and materials. The usage of ultrasonic waves for monitoring purposes is investigated since 1960s [1]. The ultrasonic testing methods are divided into the active guided wave and the passive Acoustic Emission (AE) approaches.

For the guided wave method ultrasonic waves are generated and measured by piezoelectric transducers. The differences in time and frequency domain between the generated and measured signals are analyzed and contain information about defects like cracks, corrosion, or variations in material thickness.

(a) Asymmetric mode (b) Symmetric mode

Figure 1: Lamb wave modes

Piezoelectric transducers are used only for measurement in the AE method which allows continuous in-situ monitoring. The ultrasonic waves are generated by the material itself. When a mechanical threshold is exceeded, energy is released as ultrasonic waves. The analysis of the measured waves enables classification and localization of the actual state of the system including changes resulting from underlying damages.

Monitoring remote and sophisticated systems or plants can improve the operation efficiency. For offshore wind farms, longer downtimes are observed because of their remote location and weather dependent accessibility. The energy production costs are therefore mainly driven by the maintenance costs [2]. To improve the efficiency downtime and maintenance costs must be decreased by developing new maintenance strategies [3]. Today, carbon fiber reinforced plastics (CFRP) are widely used as a replacement for metals, because the of the material's high strength to weight ratio and chemical resistance. On the other side composites material show a non-ductile behavior, therefore SHM is required for monitoring tasks. In CFRP four damage mechanism can be observed, namely delamination, matrix crack, debonding, and fiber breakage. The frequency of the damages' AE signature is concurring reported in a range of 20 to 500 kHz [4][5][6]. Additionally to the frequency spectrum of AE signals resulting from damages, the mode of the signal can be used to differentiate between damage types [7][8].

The propagation of ultrasonic waves in solids highly depends on the material and its dimensions. In thin-walled or plate-like structures the occurring ultrasonic waves are called Lamb waves. These waves have two modes, the asymmetric mode (figure 1a) and the symmetric mode (figure 1b). The symmetric mode is characterized by oscillations around the central plane while the asymmetric mode shows out of plane motion.

The propagation behavior for both modes is described as dispersive, because the propagation velocity depends on the frequency of the wave. According to the Rayleigh-Lamb frequency equation the dispersion for symmetric modes is described by

$$\frac{\tan(qh)}{\tan(ph)} = \frac{4k^2pq}{(q^2-k^2)^2} \tag{1}$$

and for asymmetric modes by

$$\frac{\tan(qh)}{\tan(ph)} = \frac{(q^2-k^2)^2}{4k^2pq}, \tag{2}$$

where p and q are derived from

$$p^2 = \left(\frac{\omega}{c_L}\right)^2 - k^2 \qquad \text{and} \qquad q^2 = \left(\frac{\omega}{c_T}\right)^2 - k^2. \tag{3}$$

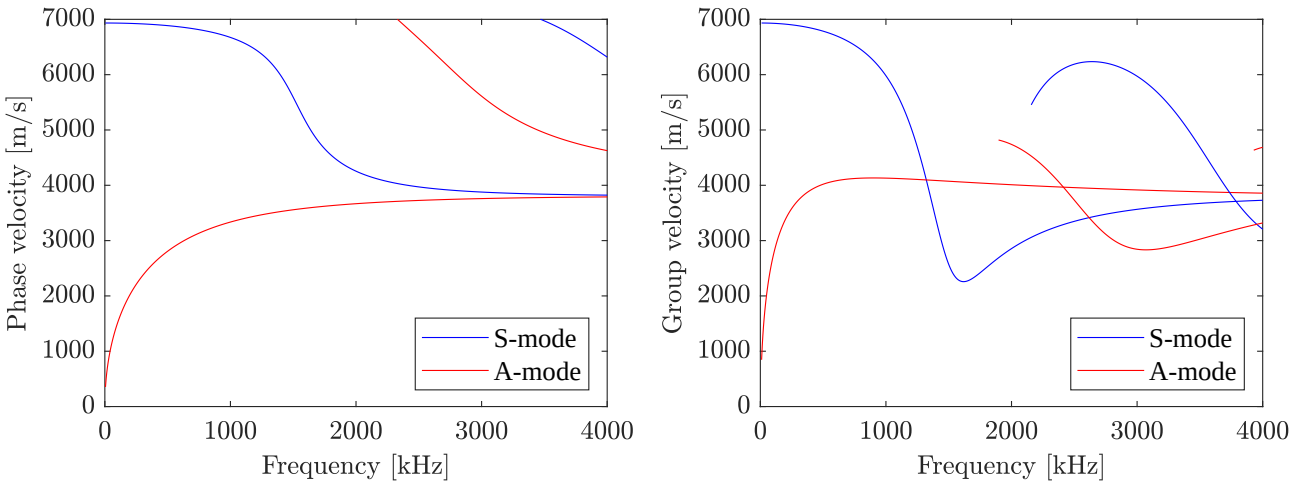

(a) Phase velocity (b) Group velocity

Figure 2: Dispersion curves for a CFRP plate with 1 mm thickness

The parameters ω, h, and k describe the angular frequency, half of the plate thickness and wave number. The wave number is calculated by $k = \omega/c_P$ where c_P denotes the wave's phase velocity, which is frequency dependent and describes the velocity of a monochromatic wave. The group velocity c_G describes the velocity of an enveloped wave group containing waves of multiple frequencies. The numerical solution of equations 1 and 2 for the parameters $E = 70.1$ Pa, $h = 1$ mm, $\rho = 1,6 \cdot 10^3$ kg m^{-3} and $\nu = 0,3$ of a quasi-isotropic CFRP plate is visualized in figure 2.

Lamb waves are reflected at material irregularities, e.g. damages and notches, and at the planar boundaries. In [9] the reflections of Lamb waves at a rectangular notch are investigated. The results show a dependency between the reflections and the ratio of the Lamb wave's wavelength to the width of the notch [9]. Xu et al. used a comparable notched specimen for their investigation of Lamb wave propagation behavior confirming the results of Lowe and Diligent [10]. In [11] reflections of Lamb waves at a hole are analyzed; the results show a dependency between the hole diameter and the measured reflections [11]. Benz et al. investigated the scattering of modes, frequency, and energy in reflections at a notched plate. The results show additionally generated modes which do not fit the theoretical solution of the slowness-frequency representation [12]. In previous publications the analysis of reflections of ultrasonic waves at material boundaries and irregularities focuses on the reflected energy. Therefore, the effects on the frequency of reflected wave is emphasized in the analysis of this contribution

This contribution is structured as follows: In section 2 the measurement chain, experimental setup, and strategy is detailed. The applied filters and signal processing methods are introduced in section 3. In section 4 the results of the experiments and data analysis are presented and discussed. Summary, conclusions, and outlook are given in section 5.

2 EXPERIMENTS AND TEST DESIGN

With the goal to isolate and analyze the reflected signal parts a suitable test design has to be generated. In the experiments a CFRP plate with the dimensions of 425 × 425 × 2 mm consisting of three CFRP-layers in 90°/0°/90° orientation is used to measure the reflections at

the boundaries of the plate. Piezoelectric transducers are used for the excitation of Lamb waves within the plate and to measure the resulting surface displacements caused by the propagating Lamb waves. The transducers' resonance frequency is 200 kHz. When attached to a surface, the resonance frequency is increased [13]. For sensing, the piezoelectric effect is utilized to transform mechanical stress to voltage and vice versa for generating Lamb waves, the inverse piezoelectric effect is used. The measurement chain is shown in figure 3. The transducers are

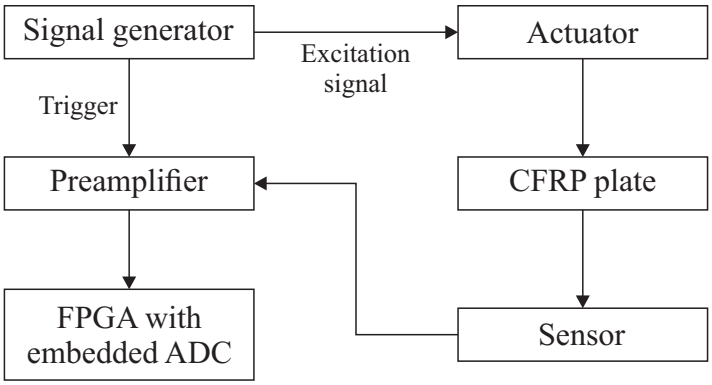

Figure 3: Measurement chain

attached to the surface of the CFRP plate in co-located pairs on both sides of the plate with a distance of 9.5 mm between the center points of the transducers used as actuator and sensor. The positions of the transducers are marked in the set ups (4). To ensure that the sensors are not affected by the sampling of the signal, a preamplifier with high input impedance and low output impedance is used. A field programmable gate array measurement board with a sampling frequency of 4 MHz and 16-bit resolution digitizes the analog voltage signal [14]. Each of the five measurement series is executed using the same CFRP plate and sensor positions. The excitation signal is generated by an arbitrary signal generator. A Hann-windowed sine signal with six cycles is used for excitation. The signal is generated with a trigger frequency 10 Hz and a peak-to-peak amplitude of 9.5 V. The sine signal's frequency is increased in steps 10 kHz starting from 10 kHz until 500 kHz. Additionally to the sensor signals the trigger signal is measured to calculate time synchronous average (TSA) during preprocessing.

The boundary conditions of the CFRP plate are varied to identify the reflections. A measurement series without varied boundary conditions is done as reference. For high attenuation and to suppress reflections the edges on both sides of the plate are covered with plasticine. Reflections are identified by the deviations between the baseline measurements and the measurements with changed boundary conditions. The fully covered setup is shown in figure 4d. The top boundary is left uncovered to investigate the reflections of acute angles, the set up is displayed in figure 4b. In figure 4c the CFRP plate is shown with an uncovered boundary on the right to isolate the reflections at a 90° angle. In the fifth setup, visualized in figure 4e, the plate's surfaces are covered with plywood which is clamped to ensure direct contact between the surfaces. In this setup a larger proportion of the plate's surface is covered to increase the attenuation effects further.

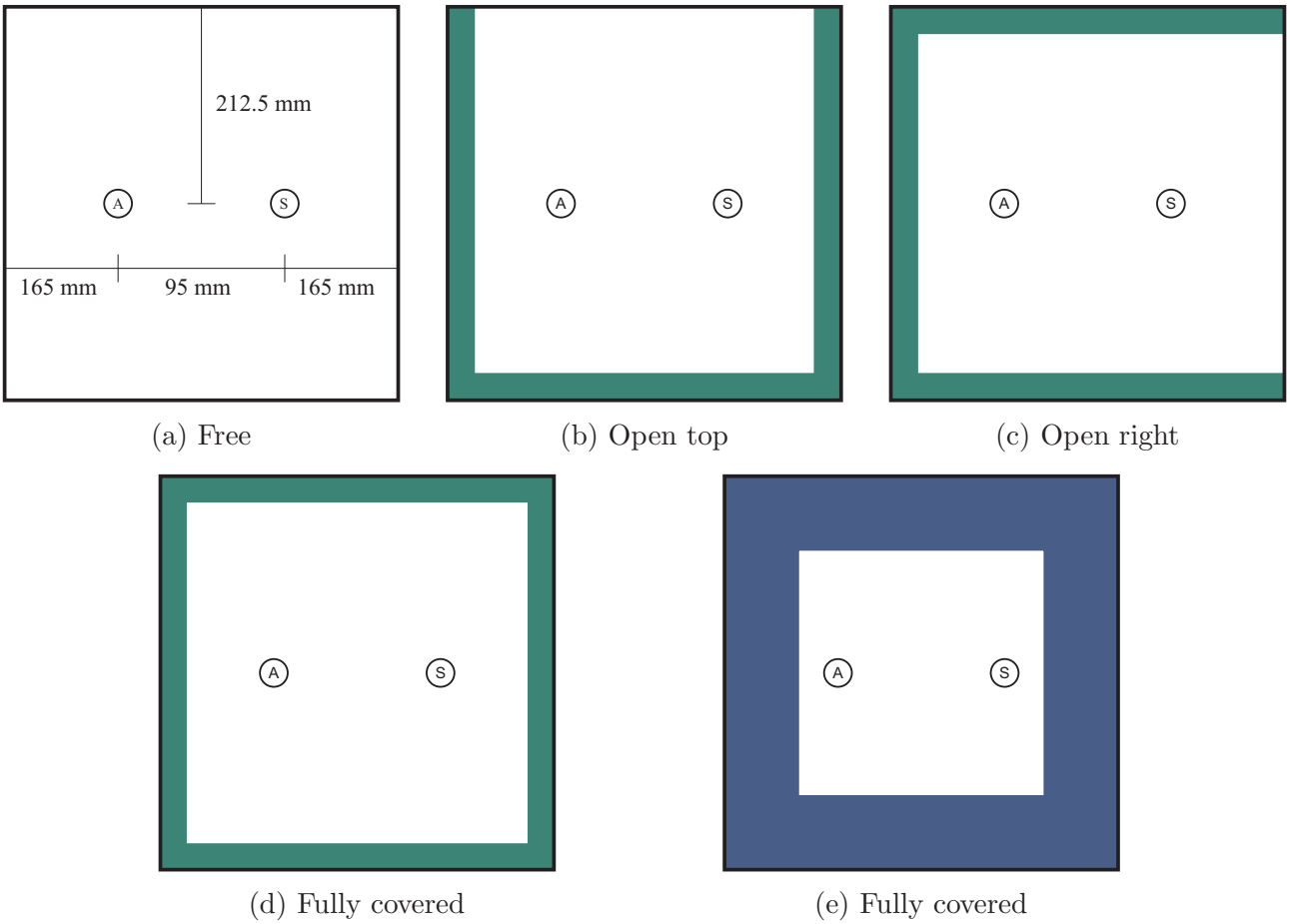

(a) Free (b) Open top (c) Open right

(d) Fully covered (e) Fully covered

Figure 4: Experimental setup

3 METHODS

The measured signals are analyzed by applying signal processing and filtering methods, which are introduced in the following sections. The reductions of noise is performed in two steps. First, a bandpass filter is applied. In the second step, based on the recorded trigger signal the TSA of each sensor signal is calculated. The TSA $m(t)$ is calculated according to

$$m(t) = \frac{1}{N} \sum_{i=0}^{N-1} x(t + iT) \tag{4}$$

for a repeating signal $x(t)$. Random Noise is reduced by factor $\frac{1}{\sqrt{N}}$ where N is the number of signal repetitions.

To analyze the frequency spectrum of a signal, the Fast Fourier transform (FFT) is performed. The Fourier transformed X_k of a discrete time signal x_n is described by

$$X_k = \sum_{n=0}^{N-1} x_n \cdot e^{-i2\pi k \frac{n}{N}}, \tag{5}$$

with $k = 0, ..., N-1$.

The representation of a signal in the time/frequency domain is determined using continuous wavelet transform (CWT). The CWT of a signal $x(t)$ is defined as

$$X_W(s,\tau) = \frac{1}{\sqrt{s}} \int_{-\infty}^{\infty} x(t) \Psi^* \left(\frac{t-\tau}{s} \right) dt \tag{6}$$

with the wavelet Ψ^*, frequency-scale parameter s and time-scale parameter τ.

The Hilbert transform (HT) enables the calculation of a signal's envelope. The transform of a real signal $x(t)$ is defined as

$$H\{x(t)\} = \frac{1}{\pi} \int_{-\infty}^{\infty} x(\tau) \frac{1}{t-\tau} d\tau. \tag{7}$$

In practice the implementation of the HT is based on the FFT and inverse Fast Fourier transform (IFFT). The analytical signal $f(t)$ is described by

$$f(t) = x(t) + \mathrm{i} H\{x(t)\} \tag{8}$$

and consist of a real and imaginary part, where the real part is the signal $x(t)$ and the imaginary part is the signal's HT $\mathrm{i}H\{x(t)\}$. The envelope $E(t)$ of the analytical signal $f(t)$ is defined as

$$E(t) = |f(t)| = \sqrt{x^2(t) + [H\{x(t)\}]^2}. \tag{9}$$

4 RESULTS AND DISCUSSION

The detection and isolation of individual waveforms are achieved by a series filters applied to the measurement signals. First, the filter proposed in [13] is applied to reduce the influence of the transducer behavior on the measurements. To generalize the approach the Min-Max-normalization is used. Local maxima are calculated in the CWT coefficients of a signal to divide the complete signal into separate windows between the local maxima. Based on the CWT coefficients the signals energy is calculated. In each separate window a local minimum is determined. If no local minimum is found, the HT is applied to the signal in the specified window to calculate a local minimum in the windowed signal's envelope. The detected local minima are used to isolate the separate signal parts.

The experimental results show different characteristic responses for synchronous and asynchronous excitation. For the asynchronous excitation the generated Lamb waves show a dominant A-mode in the frequency range of 10 to 90 kHz. In the range of 100 to 130 kHz no distinct wave pattern is observable. Between 140 and 420 kHz the S-mode is dominant. The amplitude is increasing until 260 kHz and decreases until 420 kHz where the A-mode's amplitude is surpassing up to 500 kHz.

In response to synchronous excitation the S-mode is dominant in the range of 10 to 370 kHz with the exception of 70 and 80 kHz. The amplitude is increasing until 250 kHz and decreases until 480 kHz. A waveform with A-mode is building up, first observable at 100 kHz with a continuous increasing amplitude. Starting from 380 kHz the A-mode is dominant until the end of the tested frequency range at 500 kHz.

In figures 5 and 6 the results are visualized for two examples of asynchronous excitation with 50 kHz and synchronous excitation with 350 kHz. Each of the detected signal parts is separated by a vertical line. The number above the signal is the frequency of the specific signal part and the color indicates the mode, red colored text is indicating the asynchronous mode and green

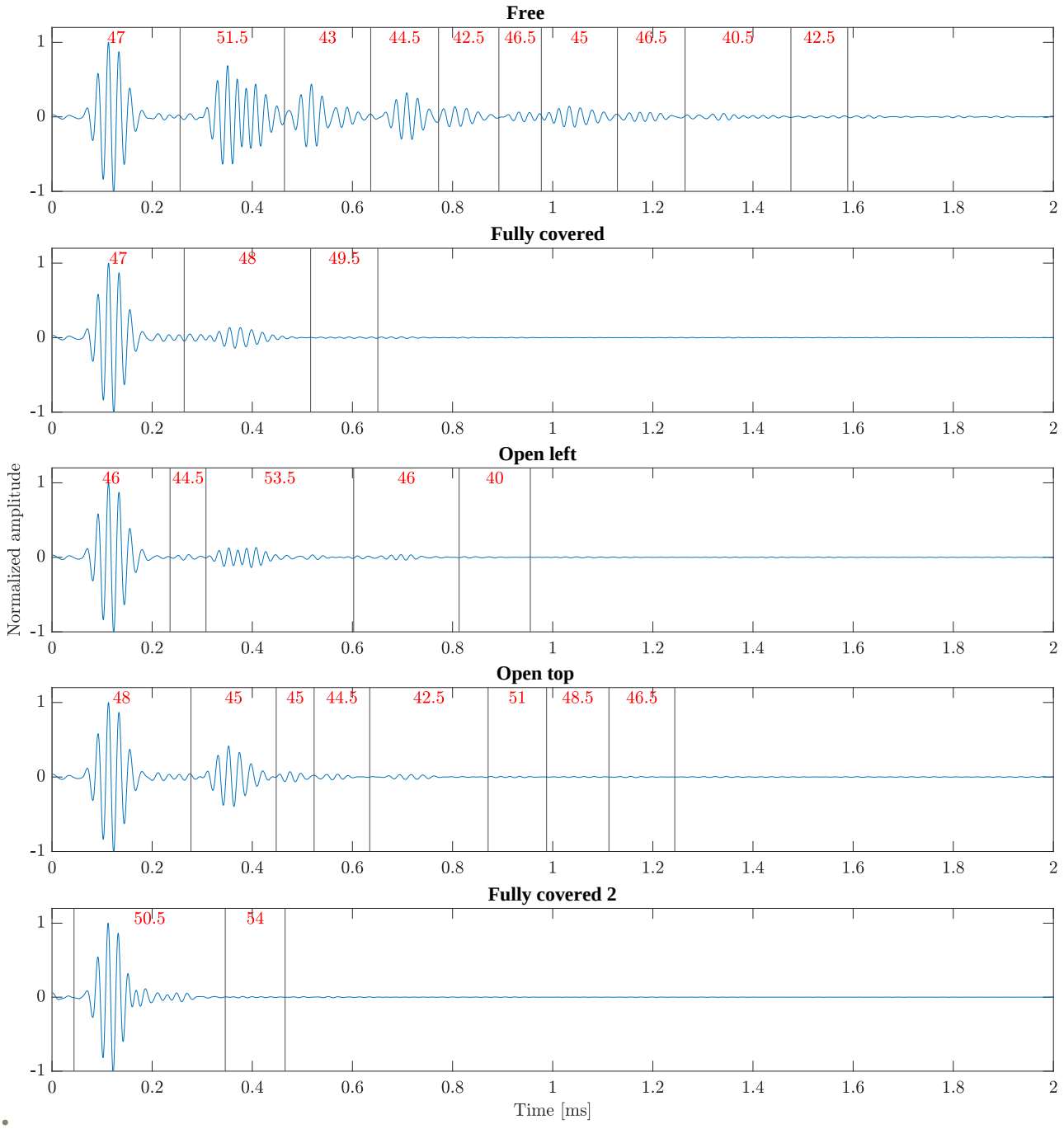

Figure 5: Measurement after asynchronous excitation with 50 kHz

colored text the synchronous mode. Throughout the entire measurements and independent of the excitation frequency the A-mode is highly affected by covered surfaces, while for the S-mode only minor changes are observable. In case of the example given in figure 5 the plot on the top shows the measurement of the undisturbed propagation. Here are, beside the initial wave at 0.15 ms, nine additional signals observable for the free boundary case. The first is centered at 0.4 ms and also detectable in measurements of fully covered edges, uncovered left edge, and uncovered top edge. The measurement of the uncovered top edge shows the highest

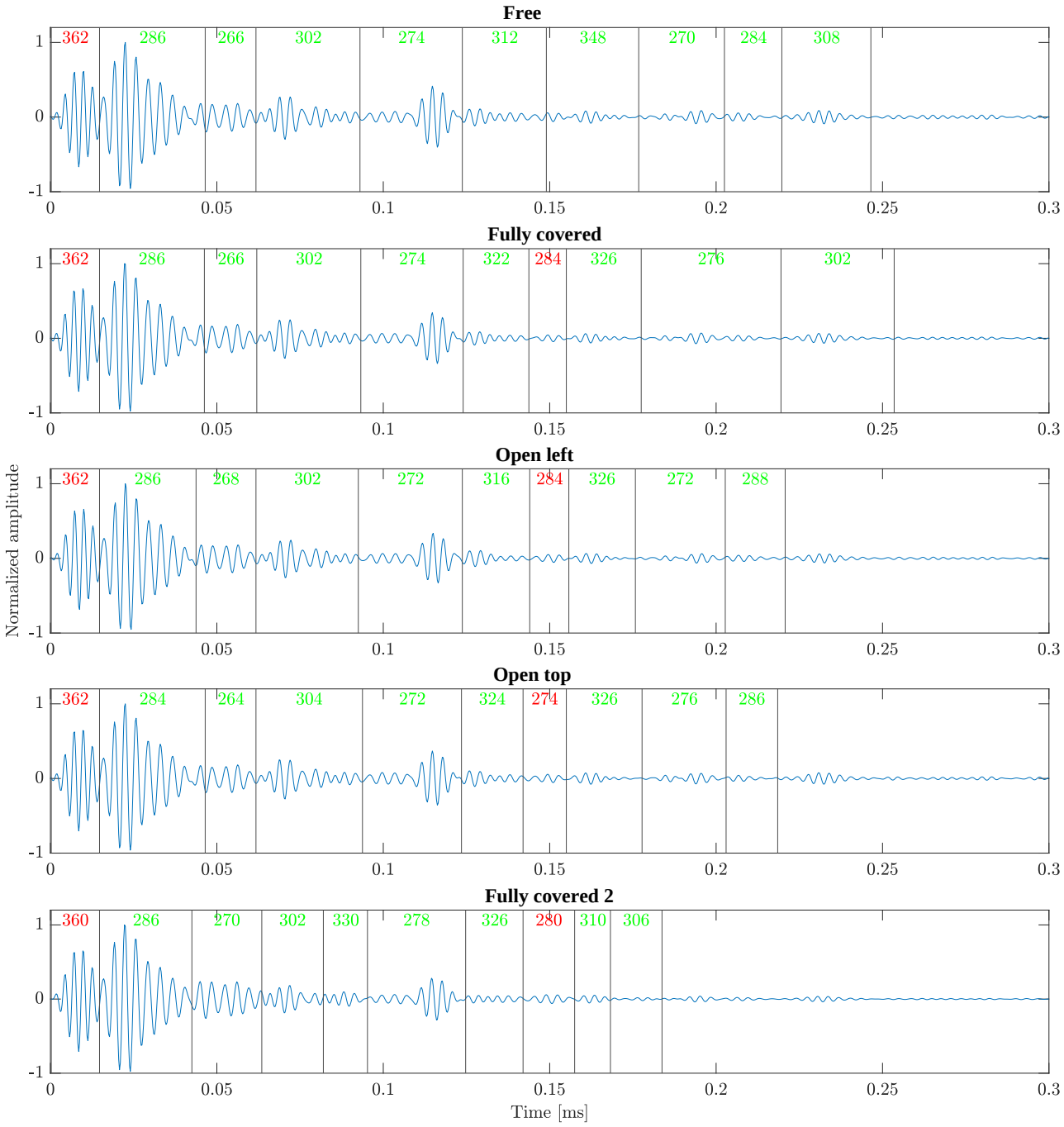

Figure 6: Measurement after synchronous excitation with 350 kHz

amplitude of the second signal part suggesting the signal is a reflection of the top edge. The evaluation of the propagation velocities shows the initial wave is traveling at 1498 $\mathrm{m\,s^{-1}}$ and the velocity of the second wave is 1448 $\mathrm{m\,s^{-1}}$. The comparison with the dispersion curves in figure 2 confirms the A-mode. The accuracy of the propagation velocity highly depends on the chosen reference points, but the similarity of the calculated velocities is an additional indicator for the top edge reflections assumption. The varied boundary conditions have a strong influence on the asynchronous mode. The comparison between the free and fully covered boundary in

figure 5 shows only two signal sections after the initial wave are detectable. For the example of synchronous excitation with 350 kHz given in figure 6 the two initial waves are detected. The first wave shows a higher frequency and asynchronous mode while the second wave has a lower frequency and synchronous mode.

In tables 1 and 2 the determined frequencies for the detected signal sections are displayed. The tables show the results for the propagation with asynchronous excitation and free boundaries as well as with synchronous excitation and fully covered boundaries. In the first column of the table the excitation frequencies are listed. The following ten columns contain the peak frequency of the first ten detected signal sections. Zero entries indicate that no signal section is detectable. For signals with asynchronous excitation at the frequency range of 400 kHz and with uncovered boundaries no signals are detectable, because the signal sections are strongly overlapping. The asynchronous excitation shows strong overlapping of waveforms with synchronous and asynchronous mode, while the signal sections generated by synchronous excitation are easier to separate.

[kHz]	1	2	3	4	5	6	7	8	9	10
20	20.2	19.2	18.2	20	18.8	17.6	21	18	16.8	18.4
40	37.6	35.6	40.4	40	34.8	35.2	39.2	37.2	36.8	38.4
60	67.8	55.8	58.2	52.2	58.8	49.8	52.2	54	54.6	0
80	78.4	78.4	72.8	73.6	70.4	64.8	79.2	79.2	80.8	78.4
100	103	87	103	102	81	102	92	90	98	100
120	112.8	136.8	127.2	136.8	129.6	129.6	122.4	99.6	134.4	134.4
140	149.8	138.6	137.2	147	140	144.2	147	142.8	141.4	137.2
160	156.8	152	187.2	158.4	145.6	142.4	164.8	147.2	144	164.8
180	180	183.6	185.4	171	196.2	189	185.4	185.4	189	187.2
200	182	192	224	206	176	206	204	222	196	196
220	254	260	246	244	254	250	254	258	222	254
240	262	254	262	258	258	268	240	262	254	260
260	260	258	252	262	266	262	264	248	264	266
280	268	260	258	268	256	264	262	270	264	252
300	268	262	258	280	270	270	264	268	296	266
320	270	264	256	304	312	272	268	266	282	296
340	304	284	266	266	250	308	318	274	272	268
360	378	324	292	274	270	354	310	318	278	290
380	366	322	348	338	356	312	308	370	384	334
400	0	0	0	0	0	0	0	0	0	0
420	478	362	518	338	378	0	0	0	0	0
440	450	524	496	452	510	428	394	460	386	414
460	464	526	508	518	520	432	418	472	512	486
480	482	530	512	514	518	426	458	470	508	508
500	470	532	516	520	526	450	462	468	516	512

Table 1: Resulting frequencies of asynchronous excitation and free boundaries

[kHz]	1	2	3	4	5	6	7	8	9	10
20	21	19.4	20	0	0	0	0	0	0	0
40	38.4	40.4	41.6	42.4	33.6	33.2	41.2	36	38.4	40
60	56.4	59.4	63.6	60	61.8	57	61.8	62.4	63.6	60.6
80	73.6	91.2	88.8	79.2	76.8	86.4	80.8	81.6	84.8	85.6
100	105	105	97	110	103	109	92	98	85	95
120	128.4	118.8	118.8	126	115.2	124.8	111.6	124.8	127.2	112.8
140	138.6	135.8	126	135.8	134.4	138.6	142.8	140	121.8	135.8
160	180.8	174.4	168	172.8	160	172.8	150.4	158.4	152	168
180	194.4	189	185.4	172.8	183.6	171	171	178.2	187.2	196.2
200	212	220	190	218	188	200	202	196	200	204
220	244	250	248	248	256	250	220	246	226	228
240	250	256	254	260	264	254	248	262	252	248
260	262	254	266	264	254	266	268	256	256	268
280	292	266	262	254	268	260	270	284	264	256
300	268	262	254	266	270	266	262	272	294	270
320	332	274	266	254	272	270	272	274	302	276
340	282	268	282	304	276	294	270	312	276	306
360	300	274	362	338	328	290	320	324	352	294
380	390	306	358	330	342	344	354	352	334	316
400	414	368	372	368	354	356	360	346	330	350
420	432	374	396	406	370	372	370	368	350	354
440	418	346	518	434	496	498	362	366	502	368
460	462	436	530	490	356	496	514	376	0	0
480	480	536	490	520	500	516	398	522	0	0
500	492	538	490	528	502	516	408	528	0	0

Table 2: Resulting frequencies of synchronous excitation and fully covered boundaries

5 SUMMARY, CONCLUSIONS, AND OUTLOOK

The combination of filters proposed in this paper is a suitable method to isolate signal sections and detect reflections. The variation of boundary conditions helps to differentiate between reflections sources. Covering the edges to suppress and allow specific reflections is an effective method for the asynchronous mode of Lamb waves. The analysis of the peak frequencies of the isolated signal sections does not show a detectable pattern of frequency changes resulting from reflections. The resulting reflections of the chosen six cycled sine wave excitation signal are of short duration, therefore the frequency analysis is subject uncertainties.

In future work larger plate dimensions could help to avoid the overlapping of multiple reflections and signal sections. In combination with an increased number of cycles of the excitation signal a more precise analysis of the frequency behavior at material boundaries is achievable.

REFERENCES

[1] Viktorov, I.A. *Rayleigh and Lamb Waves: Physical Theory and Applications*. Plenum Press, (1967).

[2] Tusar, M. I. H. and Sarker, B. R. Maintenance cost minimization models for offshore wind farms: A systematic and critical review. *International Journal of Energy Research* (2022) **46**:3739–3765.

[3] Ren, Z., Verma, A. S., Li, Y., Teuwen, J. J. and Jiang, Z., Offshore wind turbine operations and maintenance: A state-of-the-art review. *Renewable and Sustainable Energy Reviews* (2021) **144**:110886.

[4] Baccar, D. and Söffker, D., Identification and classification of failure modes in laminated composites by using a multivariate statistical analysis of wavelet coefficients. *Mechanical Systems and Signal Processing* (2017) **96**:77–87.

[5] Gutkin, R., Green, C., Vangrattanachai, S., Pinho, S., Robinson, P., and Curtis, P., On acoustic emission for failure investigation in cfrp: Pattern recognition and peak frequency analyses. *Mechanical Systems and Signal Processing* (2011) **25**:1393–1407.

[6] Hamdi, S. E., Le Duff, A., Simon, L., Plantier, G., Sourice, A., and Feuilloy , M., Acoustic emission pattern recognition approach based on Hilbert–Huang transform for structural health monitoring in polymer-composite materials. *Applied Acoustics* Applied Acoustics **74**:746–757

[7] Sause, M. G., Müller, T., Horoschenkoff, A., and Horn, S., Quantification of failure mechanisms in mode-I loading of fiber reinforced plastics utilizing acoustic emission analysis. *Composites science and technology* (2012) **72**:167–174

[8] Scholey, J. J., Wilcox, P. D., Wisnom, M. R., and Friswell, M. I., Quantitative experimental measurements of matrix cracking and delamination using acoustic emission. *Composites Part A: Applied Science and Manufacturing* (2010) **41**:612–623.

[9] Lowe, M. J. S., and Diligent, O., Low-frequency reflection characteristics of the s0 lamb wave from a rectangular notch in a plate. *The Journal of the Acoustical Society of America* (2002) **111**:64–74.

[10] Xu, H., Xu, C., and Zhou, S., Study of Lamb Wave Propagation in Plate for UNDE by 2-D FEM Model. *International Conference on Measuring Technology and Mechatronics Automation*, IEEE Computer Society, (2010) **3**:556–559

[11] Diligent, O. , Grahn, T. , Boström, A.,Cawley, P., and Lowe, M. J. S., The low-frequency reflection and scattering of the S0 Lamb mode from a circular through-thickness hole in a plate: Finite Element, analytical and experimental studies. *Journal of the Acoustical Society of America* (2002) **112**:2589–2601

[12] Benz, R., Niethammer, M., Hurlebaus, S., and Jacobs, L. J., Localization of notches with Lamb waves. *The Journal of the Acoustical Society of America* (2003) **114**:677–685

[13] Liebeton, J., and Söffker, D., Practical Experiences to Know Making Acoustic Emission-Based SHM Successful. *European Workshop on Structural Health Monitoring* (2022) **270**:812–819.

[14] Dettmann, K.-U. *Probabilistic-based method for realizing safe and reliable mechatronic systems*. https://duepublico2.uni-due.de/receive/duepublico_mods_00027251. (2012)